Indian Journal of Engineering & Materials Sciences
Vol. 27, April 2020, pp. 382-388

Ductile fracture and microstructure of a bearing steel in hot tension

Yuanming Huo[a*], Tao He[a], Yong Xue[b], Menglan Shen[a], Wanbo Yang[a] & Yujia Hu[a]

[a]School of Mechanical and Automotive Engineering, Shanghai University of Engineering Science, Shanghai 201620, China

[b]School of Material Science and Engineering, North University of China, Taiyuan 030051, China

Received: 28 September 2018; Accepted: 20 March 2020

Ductile fracture, such as micro-cavities and micro-voids, inevitably exist and evolve under tensile stress state in metal forming. Ductile fracture sways the mechanical performance of 52100 bearing steel. It is necessary to investigate the influences of strain rate and deformation temperature on both ductile fracture and microstructure evolution. Uniaxial hot tension tests were performed, in which specimens were stretched to failure in the temperatures range from 950 °C to 1160 °C and in the strain rates range from 0.01 /s to 1.0 /s. Specimens metallographies have been explored after hot tension. Experimental results show that the peak stress decreases when deformation temperature increases and strain rate decreases. The critical strain of stress–strain relationships increases when strain rate increases. Fracture morphology is severe at higher deformation temperatures and lower strain rates. Hot tension deformation capacity is worst at 1160 °C and a strain rate of 0.01 /s, has been caused by a larger and coarser grain structure.

Keywords: 52100 Bearing steel, Ductile fracture, Microstructure evolution, Hot tension, Metallography

Introduction

During hot metal forming, static and dynamic grain growth is significant in the process of dynamic recrystallization, especially as the deformation temperature increases. It is difficult to rotate and slip for coarse grains during hot bulk forming. Some micro-cavities, *i.e.* one kind of ductile damage, can inadvertently occur and subsequently evolve in coarse grain boundary, particularly under tensile stress states, *e.g.* wire drawing and extrusion, *etc*[1,2]. Except for micro-cavities in grain boundary, plasticity damage may simultaneously exist in hot bulk forming. Plasticity damage usually was found around the impurity, such as titanium nitride, manganese sulfide and aluminum oxide, *etc*. Micro-voids, *i.e.* plasticity damage, which come from debonding between matrix and impurities under the state of tensile stress and/or shear stress. Whatever micro-cavities and/or micro-voids can reduces the mechanical performance and fatigue strength[3]. It is vital to investigate the formation mechanism of ductile fracture and microstructure evolution of 52100 bearing steel during hot bulk forming.

Many articles about ductile fracture have been previously published. And, various modeling approaches were adopted to describe the evolution of ductile damage of metal. In earlier studies, some researches proposed the fracture criterion model, by considering the maximum principal stress and the mean stress. Cockcroft & Latham model[4], Oyane model[5], Ayada model[6] and Brozzo model[7,8] were classical representatives of fracture criterion model. Gurson[9], Tvergaard and Needleman[10,11], Nielsen and Tvergaard[12] inspired the microscopic damage mechanics models, which regarded ductile fracture evolution as the process of ductile damage nucleation, growth and gather to failure. The void-based Gurson-Tvergaard-Needleman (GTN) plasticity theory has attracted many attentions to its application in FE prediction[13]. Afterwards, continuum damage mechanics (CDM) based models (Lemaitre[14], Bonora[15], Bai and Wierzbicki[16], Mohr and Marcadet[17], TS Cao[18,19], Jianguo Lin[20] and Hongchao Ji[21], Sung-ju Park[22,23]) coupled the evolution rate of damage variable into the visco-plasticity constitutive model frame, which mostly considered the stress triaxiality and Lode angle parameter as the key factors during damage modeling. CDM has clear physical meaning and well predicting accuracy for the ductile fracture during bulk and/or sheet forming. Nowadays, related reports on ductile fracture and microstructure of 52100 bearing steel in hot tension are rarely found. In addition, effects of deformation temperatures and strain rates on ductile fracture and microstructure evolution need to be clarified.

*Corresponding author (E-mail: huo4023@hotmail.com)

The aim of this work was to investigate ductile fracture and microstructure evolution of 52100 steel in hot tension. Hot tension tests and metallographic experiments were carried out to investigate the deformation behavior and fracture characteristics of the steel. The effects of deformation temperature and strain rate on ductile fracture and grain structure were analyzed.

Hot Tension Tests

A bearing steel 52100 belongs to high-carbon chrome steel having the composition: C 1.01%; Si 0.25%; Cr 1.52%; Mn 0.36%; P 0.018%; S 0.003%. The initial microstructure was composed of blocky grain structures and numerous carbide particles. Hot tension testing was carried out using a Gleeble-1500D thermo-mechanical simulator to measure flow stress and study fracture characteristics. Figure 1 shows the experimental equipment, operating device and tension specimen with its size. The details regarding the types of equipment used during the experiment e.g. extensometer, thermocouples (specifications) and experimental setup diagram were exhibited in the Fig. 1. Specimens were prepared to a long cylindrical with diameter of 10 mm and length of 120 mm. Thermocouples were welded onto the surface of these specimens at their center, shown in Fig. 1(c), so that deformation temperatures could be accurately controlled. The uniform temperature section (UTS) was located near the center of each specimen. The initial UTS length was defined as 10 mm. To measure stress–strain relationships during hot tension, an extensometer was installed to record the size change of the UTS within the specimens.

Figure 2 shows the experimental procedure of hot tension. The UTS of specimens was heated to 980 °C with 10 °C /s, and then heated to 1000 °C with 2 °C /s to avoid overheating. Specimens were then held for 3 min to obtain complete austenitization, and then heated successively to 950 °C, 1020 °C, 1090 °C and 1160 °C. The specimens were then stretched to failure at 0.01 /s, 0.1 /s, and 1.0 /s. After hot tension, the specimens were quickly water-quenched to freeze the microstructure.

The microstructures of the tensioned specimens were investigated to reveal formation mechanism of ductile damage. Longitudinal section of specimens was prepared by line cutting machine. And, it was grounded coarsely and finely on grinding machine, and then polished on polishing machine. Each specimen was then etched to visualize the microstructure, using an etchant prepared using 80 ml water, 0.2 ml H_2O_2, 0.5 g sodium dodecyl benzene sulfonate (SDBS), and 2.9 g saturated picric acid that had been heated to 50–70 ℃ for 2 min. After etching, specimens were cleaned using ultrasonic oscillator. Micrographs were captured using an optical microscope. Grain structure was observed and the value of grain size was counted.

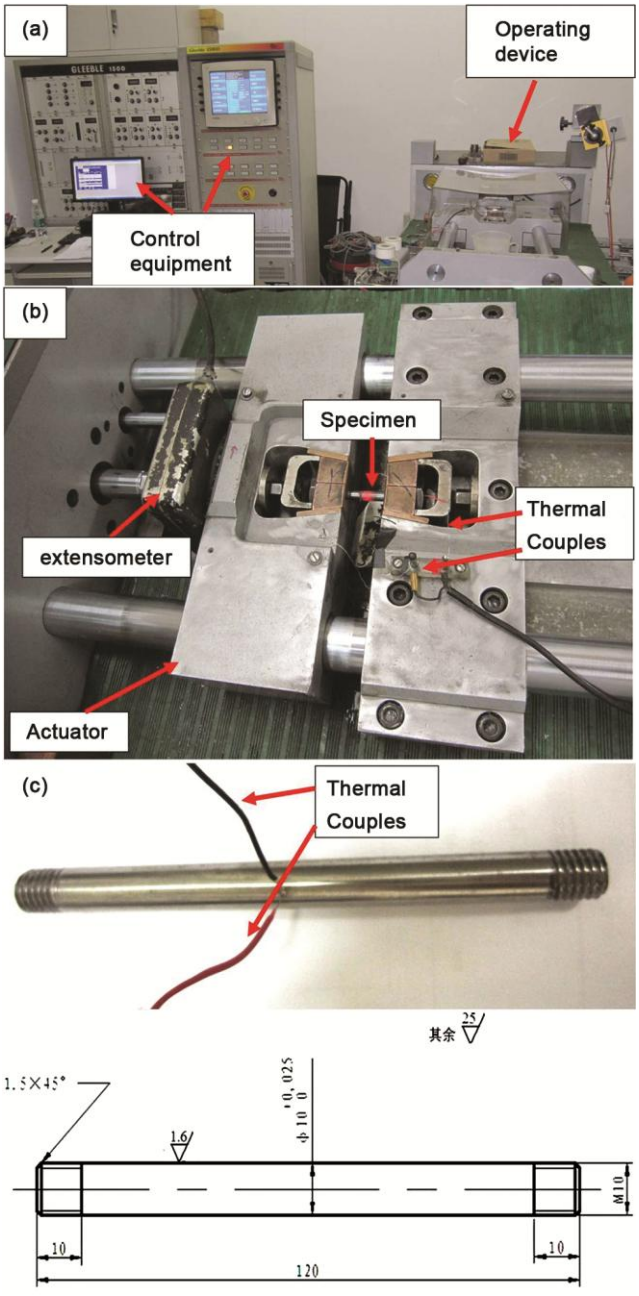

Fig. 1 — (a) Experimental equipment, (b) Operating device of hot tension and (c) Tension specimen with its size.

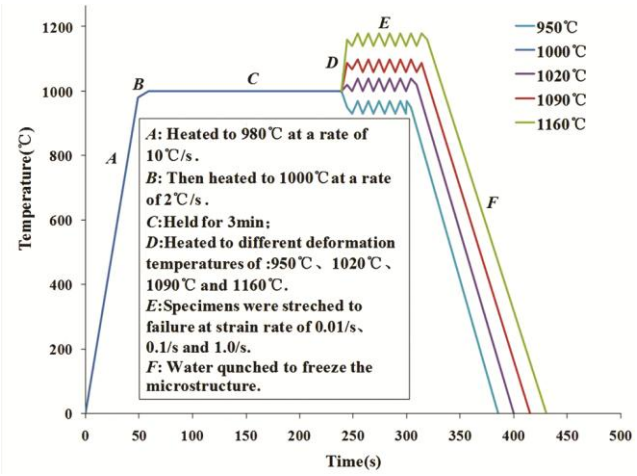

Fig. 2 — Experimental procedure of hot tension.

Results and Discussion

3.1 Hot Tension Deformation Behavior

Figure 3 shows the true stress–strain relationships under selected deformation temperatures (950 °C, 1020 °C, 1090 °C, and 1160 °C) at 0.01 /s, 0.1 /s, and 1.0 /s. The peak stress level decreases when deformation temperature increases and strain rate decreases. The minimum peak stress was about 27 MPa at 1160 °C and a strain rate of 0.01 /s; the maximum peak stress appeared at 950 °C and a strain rate of 1.0 /s, *i.e.*, 145 MPa. When the deformation temperature decreased by 70 °C, from 1160 °C to 1020 °C, the peak stress improved by about 20 MPa; a decrease in deformation temperature from 1020 °C to 950 °C improved the peak stress by about 35 MPa. When strain rate was improved from 0.01 /s to 0.1 /s or from 0.1 /s to 1.0 /s, peak stress improved by 30 MPa for a given deformation temperature.

All stress–strain curves in Fig. 3 changed with the microstructural evolution of the phases present, according to the following steps: (1) dislocation multiplication due to slipping and climbing; (2) microstructure recovery at high temperature; (3) recrystallization and grain growth; (4) micro-damage nucleation, growth, and aggregation to fracture[20,24]. Strain must exceed the critical strain value before recrystallization can take place[25]. The critical strain is constant with the variation of temperature at a given strain rate. Figure 3(a) shows that the critical strain of the stress–strain curves under different temperatures had the same value, *i.e.*, 0.12, at a strain rate of 0.01/s; Similarly, critical strain was about 0.2 at the different temperatures under 0.1/s (Fig. 3(b)); when strain rate was 1.0/s, critical strain was about 0.3 (Fig. 3(c)). The

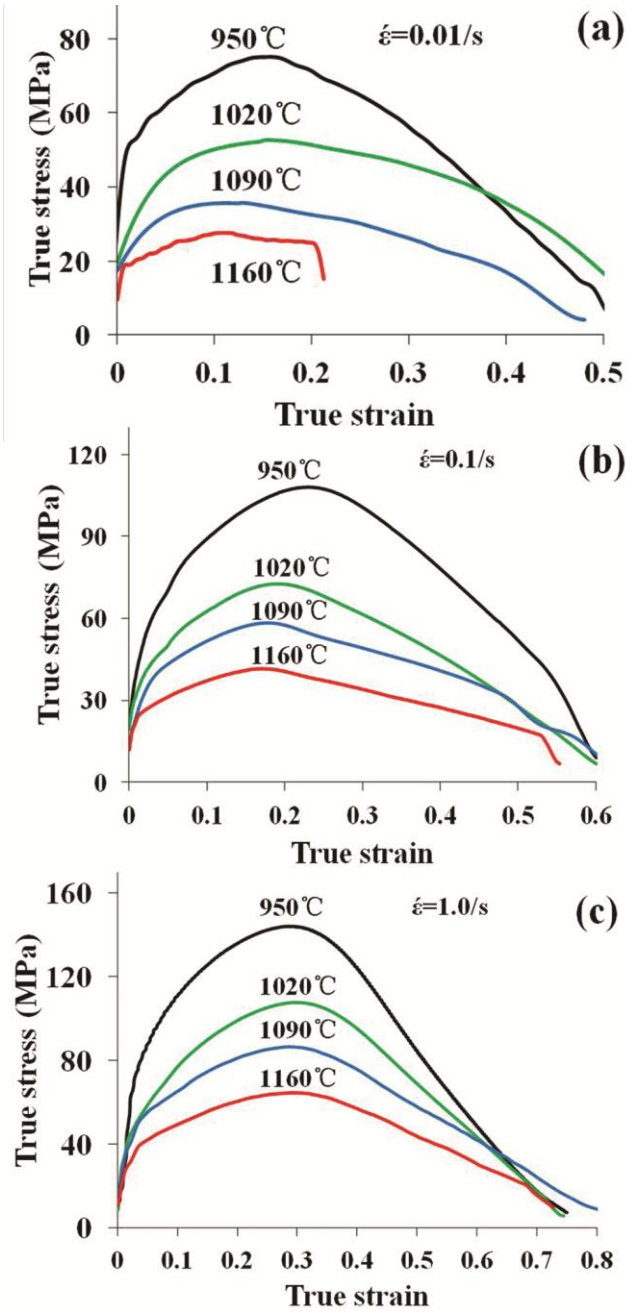

Fig. 3 — True stress-strain curves of 52100 steel at selected deformation temperatures of (950 °C, 1020 °C, 1090 °C and 1160 °C) under (a) 0.01 /s, (b) 0.1 /s and (c) 1.0 /s.

critical strain therefore increased with the increase in strain rate during hot tension.

Figure 4 shows the variations of strain to failure (STF), elongation to fracture (ETF), and reduction of area (ROA) with deformation temperature and strain rate. These parameters reflect the ductile deformation capacity of 52100 steel under different conditions. STF, ETF, and ROA decreases when deformation

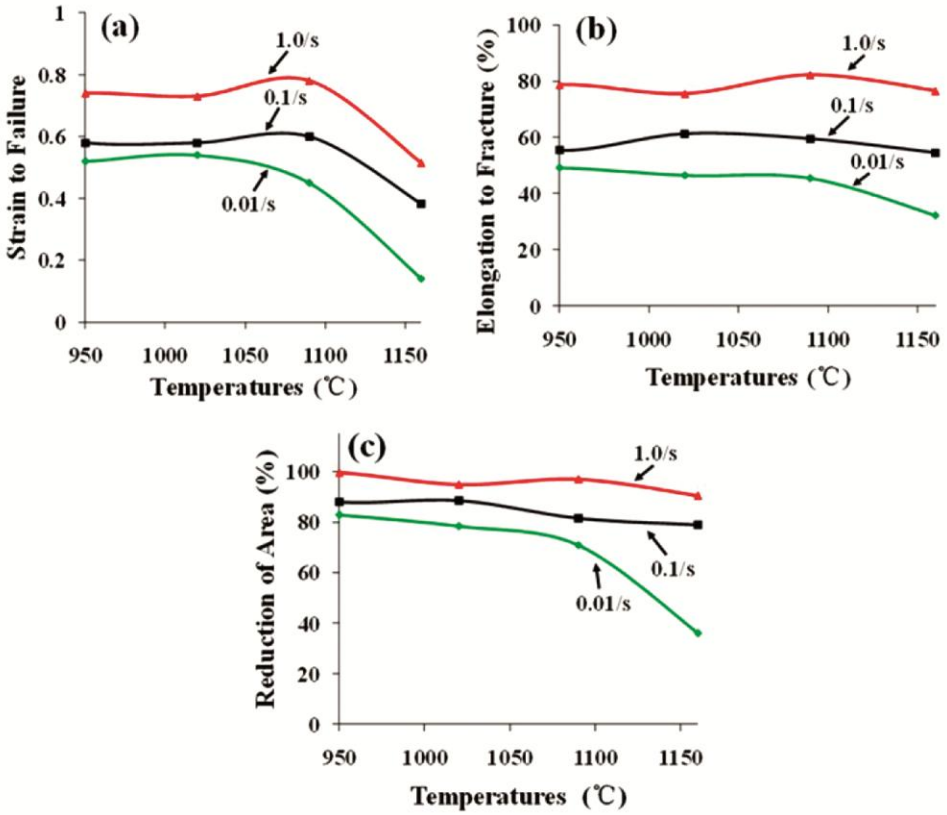

Fig. 4 — Variation of (a) STF, (b) ETF and (c) ROA with the deformation temperature and strain rate.

temperature increases and strain rate decreases. The differences were smallest between 950 °C and 1020 °C at 0.01 /s, 0.1 /s and 1.0 /s; the differences were larger for the three parameters from 1020–1160 °C at 0.01 /s, 0.1 /s and 1.0 /s.

Under 1160 °C and 0.01 /s, STF, ETF, and ROA were 0.16, 32.2%, and 36%, respectively; at 950 °C and a strain rate of 1.0 /s, the values were approximately 0.75, 76%, and 98%, respectively. This indicates that ductile deformation capacity was lowest at 1160 °C and 0.01 /s.

3.2 Effects of Deformation Temperature and Strain Rate on Ductile Fracture

Table I shows the fracture morphology at the different deformation temperatures and strain rates. The fracture diameter increases when deformation temperature increases and strain rate decreases. The fracture morphology for specimens after hot tension was severe at higher deformation temperatures and lower strain rates. At 1160 °C and a strain rate of 0.01 /s, the fracture morphology was roughest and the fracture diameter the largest. At 950 °C and 1.0 /s, the fracture tip was sharp after tension. This indicates that ductile deformation capacity was best at 950 °C and 1.0 /s, but worst at 1160 °C and a strain rate of 0.01 /s.

Table 1 — Macro-fracture morphology after tension deformation.

Temperatures (℃)	Strain rates (/s) 0.01	0.1	1.0
950			
1020			
1090			
1160			

Figure 4 and Table 1 show that the variation of fracture morphology is consistent with that of ductile deformation capacity with deformation temperature and strain rate. To account for this, grain structure

was investigated under different deformation temperatures and strain rates.

3.3 Effects of Deformation Temperature and Strain Rate on Microstructure

Figure 5 shows micrographs of 52100 steel of STF at 1.0 /s under deformation temperatures of 1020 °C, 1090 °C, and 1160 °C. For deformation at 1020 °C, the average grain size was smallest, *i.e.*, 24.8 μm (95% CI = 21–28 μm; n = 300), as shown in Fig. 5(a). For deformation at 1090 °C, the average grain size was 36.6 μm (95% CI = 34–38 μm; n = 300), as shown in Fig. 5(b). At 1160 ℃, the average grain size was largest, *i.e.*, 58.3 μm (95% CI = 53–62 μm; n = 300), as shown in Fig. 5(c). The average grain size increased at 1.0 /s when temperature was elevated from 1020 °C to 1160 °C. This indicates that the average value of grain size increases when deformation temperatures increases in this temperature range for a given strain rate.

Figure 6 shows micrographs of STF at 0.01 /s, 0.1 /s, and 1.0 /s under 1160 ℃. At 0.01 /s, the average value of grain size was largest, *i.e.*, 74.9 μm (95% CI = 69–76 μm; n = 400), seen from Fig. 6(a); At 0.1 /s, the average grain size was 69.2 μm (95% CI = 65–74 μm; n = 400), as shown in Fig. 6(b); at a strain rate of 1.0 /s, the average grain size was 58.3 μm (95% CI = 53–62 μm; n = 400), as shown in Fig. 6(c). This indicates that the average grain size decreased with an increase of strain rate from 0.01 /s to 1.0 /s at a deformation temperature of 1160 °C.

Because micrographs were obtained from specimens at STF, some micro-voids were observed in Figs. 5 and 6. Two types of ductile micro-damage often occur in hot metal forming, *i.e.*, grain boundary damage and plasticity-induced damage[22,26]. Grain boundary damage easily takes place when metal deformed at lower strain rates and higher deformation temperatures; plasticity-induced damage takes place around the second phase at higher strain rates and lower deformation temperatures[23,27]. A critical grain size of about 20 μm can be used to differentiate these two types of ductile micro-damage[28]. Figures 5 and 6 shows that the average grain size was larger than 20 μm and the grain structure was coarsest at 1160 °C and 0.01 /s. Under the lower strain rate of 0.01 /s, dynamic recrystallization was inferior and grain growth dominated at elevated temperatures, *i.e.*, grain growth led to larger grain sizes at lower strain rates. Grain boundary micro-damage therefore caused fracture failure after hot tension of 52100 steel, especially at lower stain rates and higher temperatures. The larger and coarser grain structure was the main reason for the poor deformation

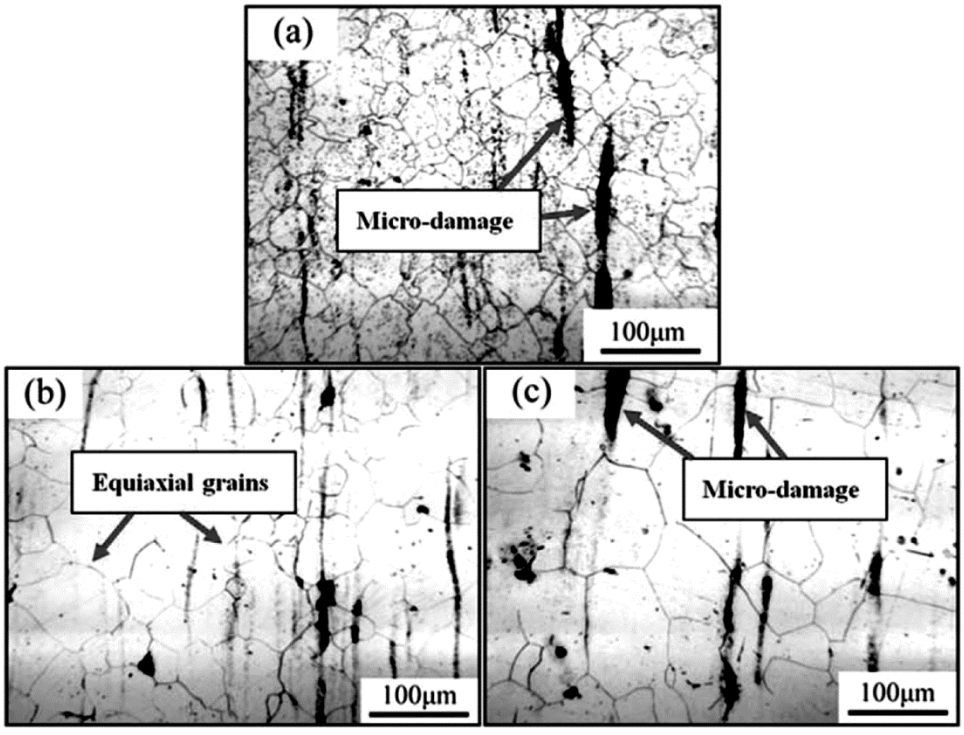

Fig. 5 — Micrographs of STF under (a) 1020 °C, (b) 1090 °C and (c) 1160 °C at 1.0 /s.

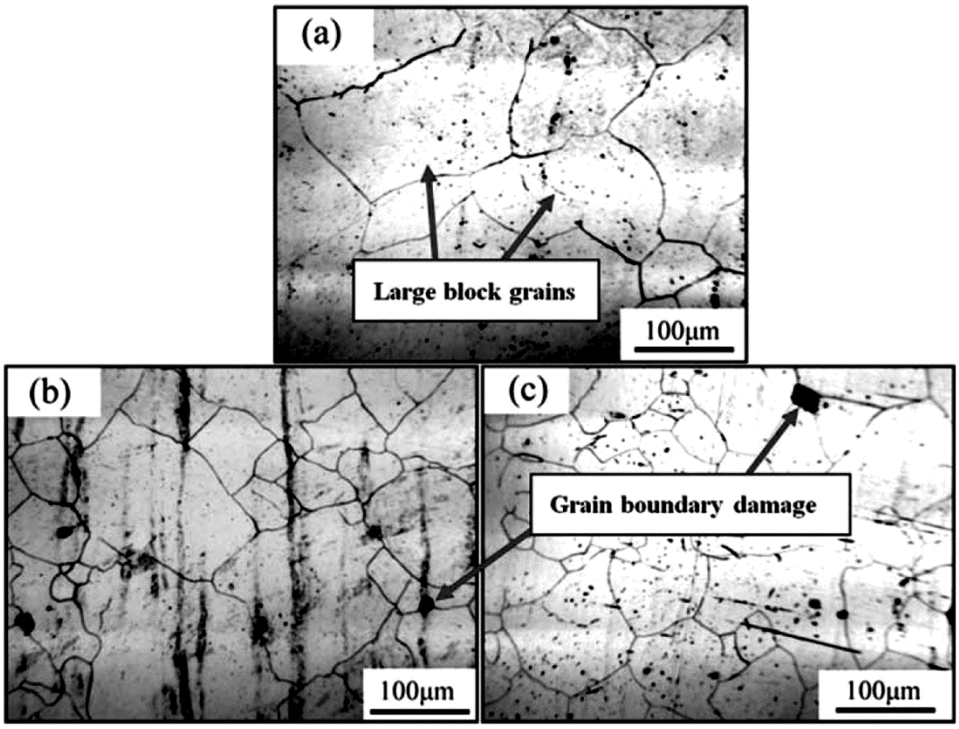

Fig. 6 — Micrographs of STF at (a) 0.01 /s, (b) 0.1 /s and (c) 1.0 /s under 1160 °C.

capacity during tension at higher temperatures and lower strain rates.

Conclusions

(i) The peak stress of 52100 steel decreases during hot tension when deformation temperature increases and strain rate decreases. The critical strain for stress–strain relationships increased with increasing strain rate during hot tension. Strain to failure, elongation to fracture, and reduction of area after hot tension decreases when deformation temperature increases and strain rate decreases.

(ii) Fracture diameters of specimens after hot tension increases when deformation temperature increases and strain rate decreases. Fracture morphology was severe for 52100 steel at higher deformation temperatures and lower strain rates. Hot tension deformation capacity was worst at 1160 °C and 0.01 /s.

(iii) The average grain size increases when deformation temperature increases and strain rate decreases. Grain structure was coarsest at 1160 °C and a strain rate of 0.01 /s. Grain growth led to larger grain sizes at lower strain rates. Grain boundary micro-damage caused fracture failure in hot tension of 52100 bearing steel, especially at lower strain rates and higher temperatures. The larger and coarser grain structure is the main reason for poor deformation capacity during tension at higher temperatures and lower strain rates.

Acknowledgments

This project is funded by the National Natural Science Foundation of China (Grant No. 51805314), National Key Research and Development Program of China (Grant No. 2018YFB1307900), Shanghai Science and Technology Commission (Grant No. 16030501200).

References

1 Bai Q, Mohamed M, Shi Z, Lin J & Dean T, *Int J Adv Manuf Tech*, 88 (2017) 10.

2 Zhu Y, Engelhardt M D & Pan Z, *Acta Mech Sinic*, 035 (2019) 600.

3 Lin Y C, Liu Y X, Liu G, Chen M S & Huang Y C, *J of Mater Eng Perform*, 24 (2015) 221.

4 Terhorst M, Feuerhack A, Trauth D & Klocke F, *Int J of Mater Form*, 9 (2015) 1.

5 Oyane M, Sato T, Okimoto K & Shima S, *J of Mech Work Tech*, 4 (1980) 65.

6 Song Y U & Feng W, *Front of Mechan Eng*, 6 (2011) 308.

7 Seok D Y, Kim D, Kim S W, Bak J, Lee Y S & Chung K, *Met Mater Int*, 21 (2015) 54.

8 Ragab A R, *Metall Mater Trans A*, 37 (2006) 1281.

9 Xue Z, Faleskog J & Hutchinson J W, *Int J Solids Struct*, 50 (2013) 4258.

10 Abbasi M, Bagheri B, Ketabchi M & Haghshenas D F, *Comp Mater Sci*, 53 (2012) 376.

11 Liu X G, Wang C, Deng Q F & Guo B F, *J Iron Steel Res Int*, 1 (2019) 12.

12 Nielsen K L & Tvergaard V, *Eng Fract Mechan*, 77 (2010) 1031.

13 Kiran R & Khandelwal K, *Fatigue Fract Eng M*, 37 (2014) 171.

14 Azinpour E, Ferreira J P S, Parente M P L & Cesar de Sa J, *Adv Model Simu in Eng Scien*, 5 (2018) 24.

15 Bonora N & Ruggiero A, *Int J Solids Struct*, 42 (2005) 1401.

16 Bai Y & Wierzbicki T, *Int J Plasticity*, 24 (2008) 1071.

17 Marcadet S J & Mohr D, *Int J Plasticity*, 72 (2015) 21.

18 Cao T S, Bobadilla C, Montmitonnet P & Bouchard P O, *J Mater Process Tech*, 216 (2015) 385.

19 Cao T S, Gachet J M, Montmitonnet P & Bouchard P O, *Eng Fract Mech*, 124-125 (2014) 80.

20 Cai Z, Ji H, Pei W & Huang X, *Results Phys*, 15(2019) 102.

21 Lin J, Liu Y & Dean T A, *Int J Damage Mech*, 14 (2005) 299.

22 Park S J, Lee K, Cerik B C & Choung J, *Ships Offshore Struct*, 1 (2019) 12.

23 Park S J, Lee K, Choung J & Walters C L, *Ships Offshore Struct*, 1 (2018) 11.

24 Sancho A, Cox M J, Cartwright T, Aldrich-Smith G D, Hooper P A, Davies C M & Dear J P, *Procedia Struct Integrity*, 2 (2016) 966.

25 Lin J, Liu Y, Farrugia D C J & Zhou M, *Philos Mag*, 85 (2005) 1967.

26 Li N, Sun C, Guo N, Momhamed M, Lin J & Takeki M, *Procedia Eng*, 81 (2014) 1744.

27 Mohamed S M, Foster A D, Lin J G, Balint D S & Dean T A, *Int J Mach Tool Manu*, 53 (2012) 27.

28 Lin J, Foster A D, Liu Y, Farrugia D C J & Dean T A, *Eng Trans*, 55 (2007) 43.